



## Cu Electrodeposition from Methanesulfonate Electrolytes for ULSI and MEMS Applications

Maksudul Hasan\* and James F. Rohan\*\*<sup>z</sup>

Tyndall National Institute, University College Cork, Lee Maltings, Cork, Ireland

Methanesulfonic acid (MSA) is an alternative to sulfuric acid electrolyte for metal deposition. The electrochemical nucleation and growth of Cu on a glassy carbon electrode in methanesulfonate was compared with sulfate baths. The overpotential for Cu deposition was much smaller in the MSA bath compared to the traditional sulfuric acid bath, and Cu nucleation occurred at a higher rate in the MSA bath. The measured diffusion coefficient value for Cu deposition from the MSA bath was  $6.82 \times 10^{-6} \text{ cm}^2/\text{s}$ . UV-visible spectroscopic results confirmed that the coordination of Cu species was the same in both electrolytes. Cu electrodeposition on Ni sputtered Si substrate from the high efficiency MSA bath was photoresist-compatible with no void formation. One-dimensional Cu nanorods were also deposited through an anodized aluminum oxide template on a Ni evaporated seed layer substrate, showing potential applications as electrical interconnects in ultralarge scale integration (ULSI) and micro-electromechanical systems (MEMS).

© 2010 The Electrochemical Society. [DOI: 10.1149/1.3332729] All rights reserved.

Manuscript submitted December 10, 2009; revised manuscript received January 26, 2010. Published April 7, 2010.

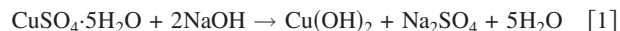
Cu is the present and future interconnect material in high end microprocessors and memory devices because of its lower electrical resistivity and higher electromigration resistance than aluminum. Dual damascene Cu electroplating is now commonly used in semiconductor devices usually employing a mixture of  $\text{CuSO}_4/\text{H}_2\text{SO}_4$ . To achieve a so-called bottom-up or superconformal deposit, various types of organic additives are also added.<sup>1,2</sup> Moreover, additives such as bis-(3-sodiumsulfopropyl disulfide) that are used as accelerators enhance the bottom-up fill capability of Cu electroplating.<sup>3</sup> The inhibiting effects of poly(ethylene glycol) (PEG) during Cu electroplating has also been studied.<sup>4</sup> PEG-Cl electrolyte that is commonly used as a suppressor in semiconductor Cu electroplating bath decomposes to PEG of smaller molecular weight at the cathode. The smaller molecular weight PEG has less adsorption ability on the electrode surface, and thus its inhibiting effect on Cu reduction decreases gradually.

In this study, we report that methanesulfonic acid (MSA) is an alternative electrolyte system that could replace sulfuric acid in practical applications. MSA is a strong electrolyte and its conductivity in water is similar to other strong acids such as sulfuric or hydrochloric acid and higher than that of other organic acids.<sup>5</sup> Nevertheless, MSA has a “green” character in two different ways. First, it is odorless and does not generate toxic gas fumes, which make it very safe to handle.<sup>5</sup> Second, it is readily biodegradable and recyclable.<sup>6</sup> Recycling of MSA is readily achieved because of its excellent solubility in water so that it can be extracted from an organic phase with small amounts of water. These result in easily treatable effluents that are less hazardous compared to all other commercial baths such as sulfate, chloride, fluoride, etc. MSA also attracts great attention because of its nonoxidant characteristics compared to other traditional electrolytes, i.e., sulfate, nitrates, etc. Additionally, MSA solutions are easy to handle because they remain in liquid form down to  $-60^\circ\text{C}$  ( $\text{H}_2\text{SO}_4:3^\circ\text{C}$ ), and they have greater thermal stability than other organic acids. The baths produce a reduced amount of waste and sludge, and thus the early investment of resources can be minimized. Nevertheless, information on the fundamental properties of such electrolytes in the “open” scientific literature is very scarce. This paper reports the basic electrochemistry of Cu metal ion deposition in aqueous MSA solution by comparison with the traditional sulfate bath. Here, we present electrodeposition of Cu on Ni sputtered Si substrate patterned using optical photolithography. We also report the fabrication of one-dimensional (1D) Cu nanorods based on the anodized aluminum oxide (AAO) medi-

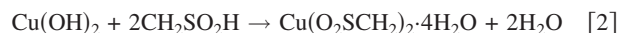
ated direct electrodeposition technique from the MSA plating bath for interconnects in ultralarge scale integration (ULSI) and micro-electromechanical systems (MEMS) applications.

### Experimental

Cu methanesulfonate was prepared as follows.  $\text{Cu}(\text{OH})_2$  was first precipitated from the sulfate solution using NaOH (excess) according to the following equation



Cu sulfate pentahydrate (31.21 g, 0.125 mol; Fisher Scientific, analytical reagent grade) was dissolved in water and slowly poured in an aqueous solution of sodium hydroxide (10 g, 0.25 mol; Sigma-Aldrich, reagent grade, 97%). The bluish slurry Cu hydroxide was washed with deionized (DI) water. The filtrate was dried in vacuo (1 mm Hg) at  $50^\circ\text{C}$  and used in the synthesis of Cu methanesulfonate. The reaction proceeds according to the following equation



The powdered Cu hydroxide (12.0 g, approximately 0.125 mol) was dissolved in MSA (24.025 g, 0.250 mol; Sigma-Aldrich, 99% anhydrous) at  $80^\circ\text{C}$  for 1 h, and enough DI water was then added to produce a homogeneous solution. The formation of Cu methanesulfonate salt was induced by isopropyl alcohol (IPA). IPA (100 mL) was poured into the above solution at  $50^\circ\text{C}$  and left overnight for crystallization, the crystalline precipitate was collected by vacuum filtration and washed with IPA and ether. The solid product was brought to constant weight in vacuum (1 mm Hg). The compound  $\text{Cu}(\text{O}_3\text{SCH}_2)_2 \cdot 4\text{H}_2\text{O}$  was characterized by ethylenediaminetetraacetic acid complexometric titration, CHN analysis (Interscience Ce Instrument EA1110).

Cu deposition/dissolution experiments were carried out in a three-electrode electrochemical cell. The working electrode glassy carbon (GC) was constructed from a 3 mm diameter vitreous carbon rod with an active surface area of  $0.0803 \text{ cm}^2$  (geometrical area:  $0.07065 \text{ cm}^2$ ). The active surface area was determined using the well-characterized ferricyanide system on the GC electrode, and the active area was determined using the Cottrell equation. The electrode surface was successively polished with 0.3, 0.1, and  $0.05 \mu\text{m}$  alumina powder (Struers) to a mirror finish and was ultrasonically rinsed before the experiment. Two equal molar solutions for these experiments consisting of 0.05 M  $\text{CuSO}_4 \cdot 5\text{H}_2\text{O}$  (Fisher Scientific, analytical reagent grade) in 1 M  $\text{H}_2\text{SO}_4$  (Air Products, 96%) and 0.05 M  $\text{Cu}(\text{O}_3\text{SCH}_2)_2 \cdot 4\text{H}_2\text{O}$  (in house) in 1 M MSA (Sigma-Aldrich, 99% anhydrous) were used. All electrochemical experiments were carried out with a CHI 660C potentiostat (CH Instruments, Inc.) coupled to a personal computer, a Ti/Pt mesh counter electrode, and a  $\text{H}_2$  reference electrode. The temperature of the cell

\* Electrochemical Society Student Member.

\*\* Electrochemical Society Active Member.

<sup>z</sup> E-mail: james.rohan@tyndall.ie

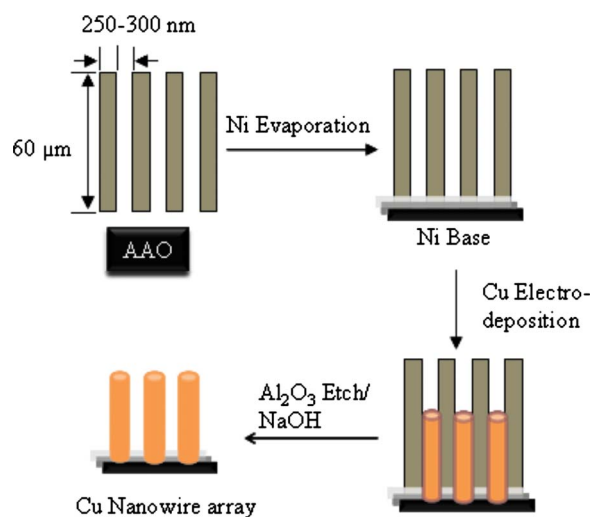


**Figure 1.** (Color online) Schematic illustration of the synthesis process of the high aspect ratio Cu nanorod arrays.

was thermostatically controlled at  $20 \pm 1^\circ\text{C}$ . Before a series of experiments, the electrolytic solution was deaerated for 2 h with high purity nitrogen, which was presaturated with water. The ultraviolet-visible (UV-vis) spectroscopy experiments of two equimolar solutions of  $0.05\text{ M Cu}(\text{O}_3\text{SCH}_3)_2 \cdot 4\text{H}_2\text{O}$  and  $\text{CuSO}_4 \cdot 5\text{H}_2\text{O}$  were carried out with a CARY 5000 spectrophotometer to compare the coordination of  $\text{Cu}^{2+}$  ions into solutions with the reference solutions of  $1\text{ M CH}_3\text{SO}_3\text{H}$  and  $1\text{ M H}_2\text{SO}_4$ , respectively.

Cu electrodeposition on Si substrates was carried out using a mask with arrays of  $(100 \times 100\ \mu\text{m})$  features and a pitch of  $400\ \mu\text{m}$ . These features were patterned in a Ni sputtered Si substrate by a photolithographic technique. A  $100\ \text{mm}$  diameter Si wafer was used as a substrate, with thin layers of Ti ( $200\ \text{\AA}$ ) and Ni ( $1000\ \text{\AA}$ ) physically deposited by the sputtering process. Here, the Ti layer improves the adhesion of Ni to the Si substrate, which acts as the conducting seed layer. A positive photoresist AZ 9260 was spun on the wafer to a height of  $12\ \mu\text{m}$ , UV exposed, and developed in an AZ 400k developer. Cu was deposited in the developed photoresist mold from  $0.1\text{ M Cu}(\text{O}_3\text{SCH}_3)_2 \cdot 4\text{H}_2\text{O} / 1\text{ M CH}_3\text{SO}_3\text{H}$  at  $20 \pm 1^\circ\text{C}$ , with the Ti/Pt mesh as a counter electrode. After electroplating, the resist was stripped in acetone; the wafer was then rinsed and dried with nitrogen. 1D nanoscale electrodeposition for noble interconnects in the three-dimensional (3D) integration of ULSI and MEMS applications was performed on commercial AAO Anodisc membranes (Whatman,  $10^9\ \text{pores}/\text{cm}^2$ ). The complete fabrication process of Cu nanorods is illustrated in Fig. 1. A  $500\ \text{nm}$  thin layer of Ni conducting layer was deposited onto one side of the AAO template by the E-beam evaporation technique (Temescal FC-2000). The electrodeposition was carried out in  $0.24\text{ M Cu}(\text{O}_3\text{SCH}_3)_2 \cdot 4\text{H}_2\text{O} / 1.8\text{ M CH}_3\text{SO}_3\text{H}$  at  $20 \pm 1^\circ\text{C}$  with a slow convection of the electrolyte at a constant current of  $40\ \text{mA}$ . Based on the available surface area on the exposed back side of the AAO ( $21\ \text{mm}$  in diameter) and in the pores of the template,  $40\ \text{mA}$  may be equated with  $6.6\ \text{mA}/\text{cm}^2$ . In a two-electrode setup, a Ti/Pt mesh was the anode and a Ni seed layer on the AAO substrate was the working electrode (cathode). A Cu wire was connected to the Ni conducting side of the template by a silver conductive paint (Radiionics Ltd., Ireland) and left to dry overnight before use. The morphology of the Cu deposits was analyzed by a scanning electron microscope (SEM, FEI Nova 630 Nano-SEM and Hitachi S-4000 at  $15\ \text{kV}$ ) and characterized by an X-ray powder diffractometer (Philips PW3710-MPD with  $\text{Cu K}\alpha$  radiation,  $\lambda = 1.54056\ \text{\AA}$ , at  $40\ \text{kV}$   $35\ \text{mA}$ ), and data were analyzed using a Philips X'pert X-ray diffraction (XRD) software.

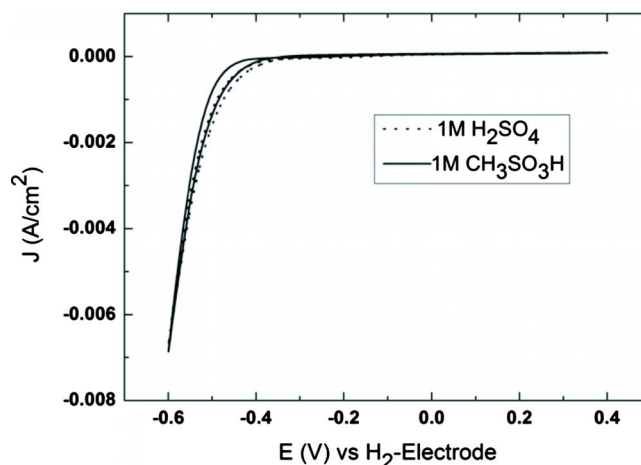


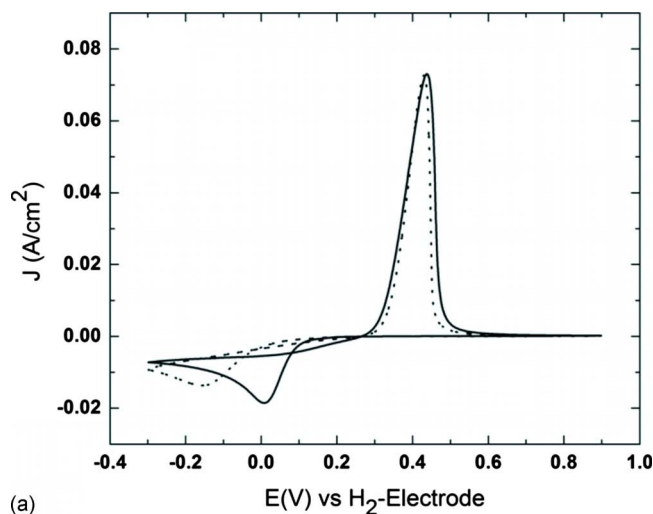
**Figure 2.** (Color online) CVs of  $1\text{ M CH}_3\text{SO}_3\text{H}$  (solid line) and  $1\text{ M H}_2\text{SO}_4$  (dotted line) on a GC disk electrode (conditioning/initial potential:  $0.4\ \text{V}$ ,  $20\ \text{s}$ ; scan rate:  $0.01\ \text{V/s}$ ).

## Results and Discussion

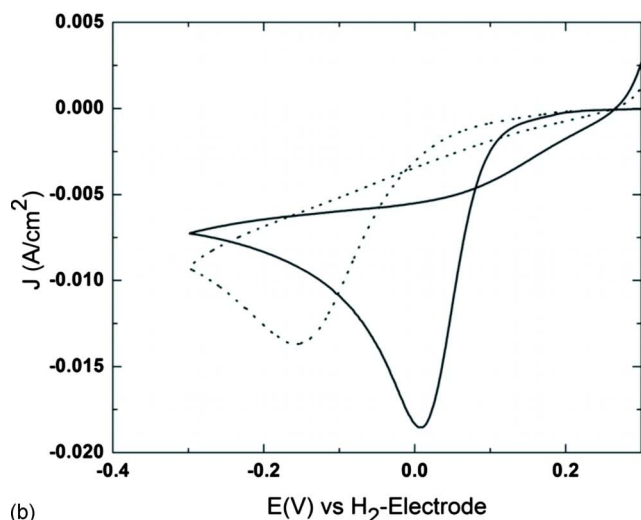
The electrochemical window of the background electrolyte of  $1\text{ M}$  aqueous MSA and sulfuric acid solutions (Fig. 2) in the cathodic direction was measured by cyclic voltammetry (CV). The small current, which remains constant over the potential interval from  $0$  to  $-0.3\ \text{V}$ , is not due to a faradaic process but is merely a capacitive current associated with the action of a continuous potential change during the CV experiment. The sharp current rise at  $-0.4\ \text{V}$  is due to hydrogen evolution. Thermodynamically, hydrogen evolution on an electrode surface can occur starting from  $0\ \text{V}_{\text{SHE}}$  (where SHE denotes standard hydrogen electrode). In this case, an overpotential of  $0.3\ \text{V}$  for hydrogen evolution reflects the activation barrier that has to be overcome for the formation of hydrogen gas on the GC electrode in the MSA bath. No electrochemical reaction on the GC electrode takes place at potentials more positive than  $-0.3\ \text{V}$ .

Figure 3a shows two cyclic voltammograms of the Cu deposition obtained from methanesulfonate and sulfate baths during the forward sweep to lower potentials. In methanesulfonate, a sharp rise at around  $0.125\ \text{V}$  is observed by comparison with  $0.05\ \text{V}$  in the sulfate bath, which passes through a maximum at around  $0\ \text{V}$ , corresponding to  $-0.160\ \text{V}$  for sulfate bath, and then decreases due to the increase in the diffusion layer thickness. In the reversed sweep, the current passes through zero at around  $0.275\ \text{V}$  before oxidation commences. This crossover potential is a good approximation of the equilibrium potential. The cathodic peak maximum is shifted by  $0.160\ \text{V}$  to a more positive potential value in methanesulfonate bath (full line) compared to the sulfate bath (dotted line), thus the critical overpotential for Cu deposition on the GC electrode is much lower in the methanesulfonate. In addition, the cathodic peak current ( $I_p = 0.019\ \text{A}/\text{cm}^2$ ) in the methanesulfonate bath is also higher than that obtained in the sulfate bath ( $I_p = 0.014\ \text{A}/\text{cm}^2$ ), implying that the amount of Cu deposit at the same potential interval and sweep rate is particularly higher in the methanesulfonate bath. The nucleation loops shown in Fig. 3b are an indication of the nucleation and growth process of Cu on the GC substrate. The initial adsorption and nucleation rate of  $\text{Cu}^{2+}$  ions at the cathode is faster compared to that in the sulfate bath. Further, on the reverse sweep, when  $E > E_{\text{eq}}$ , the anodic peak corresponding to the dissolution of Cu is observed.

CV is not always an accurate quantitative technique because the electrode potential changes continuously, and so does the kinetics for electrochemical reactions, during the time scales of the experiment.<sup>7</sup> Therefore, the kinetics of Cu deposition is also investigated by chronoamperometric experiments. Two chronoamperometric current transients from methanesulfonate and sulfate baths are shown in Fig. 4, in which the electrode potential was instanta-



(a)



(b)

**Figure 3.** (Color online) (a) CVs of Cu deposition from methanesulfonate (solid line) and sulfate (dotted line) baths on a GC disk electrode and (b) close-up view of the nucleation loops of copper deposition (conditioning/initial potential: 0.4 V, 20 s; scan rate: 0.05 V/s).

neously changed from 0.4 V (a value where no electrochemical activity occurs) to  $-0.1$  V in the overpotential deposition region. Both the transients increase through a maximum and reach the same current value at longer times. This behavior is expected for reduced species that are insoluble in the electrolyte such as in metal nucleation and phase growth. However, Fig. 4 shows that at the same potential steps, the current transient in the methanesulfonate bath is significantly steeper than that in the sulfate bath, which represents a faster nucleation rate in this bath at similar potentials.

The determination of the diffusion coefficient of  $\text{Cu}^{2+}$  ions in the methanesulfonate bath is estimated using the Cottrell equation<sup>7</sup>

$$I(t) = nFAC \left( \sqrt{\frac{D}{\pi t}} \right) \quad [3]$$

in which  $n$  is the number of electrons transferred per molecule,  $F$  is Faraday's constant (C/mol),  $A$  is the electrode area ( $\text{cm}^2$ ),  $D$  is the diffusion coefficient ( $\text{cm}^2/\text{s}$ ), and  $C$  is the concentration of the species in the solution ( $\text{mol}/\text{cm}^3$ ). A potential step was applied to the GC electrode from an initial value of 0.4 V (where no electrochemical reaction occurs) to a final value of  $-0.125$  V and held at this potential for 5 s. Afterward, the copper deposit was removed by applying an anodic potential of 0.7 V for 30 s. The measured diffu-

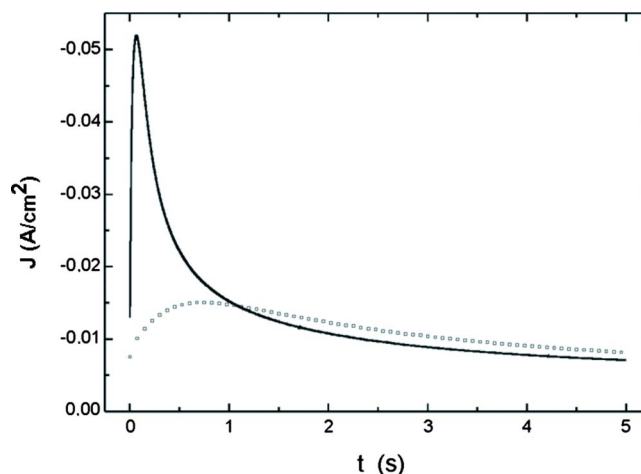
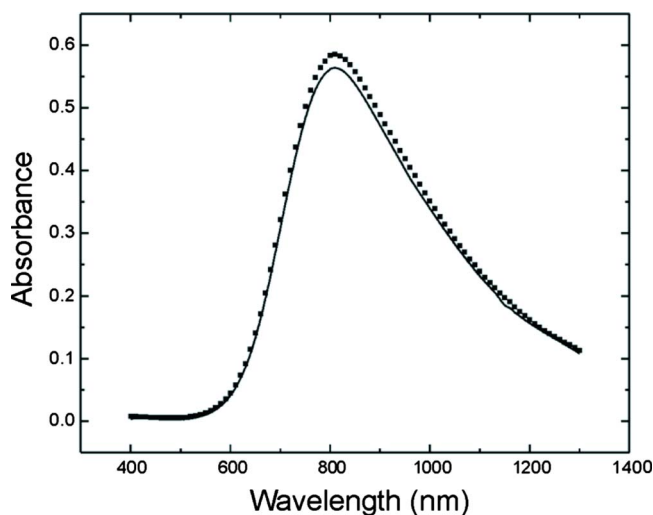


**Figure 4.** (Color online) Chronoamperograms of Cu deposition from methanesulfonate (solid line) and sulfate (square line) baths at  $-0.1$  V on a GC disk electrode (conditioning/initial potential: 0.4 V, 10 s, deposition time: 5 s). The inset is the enlarged initial time region.

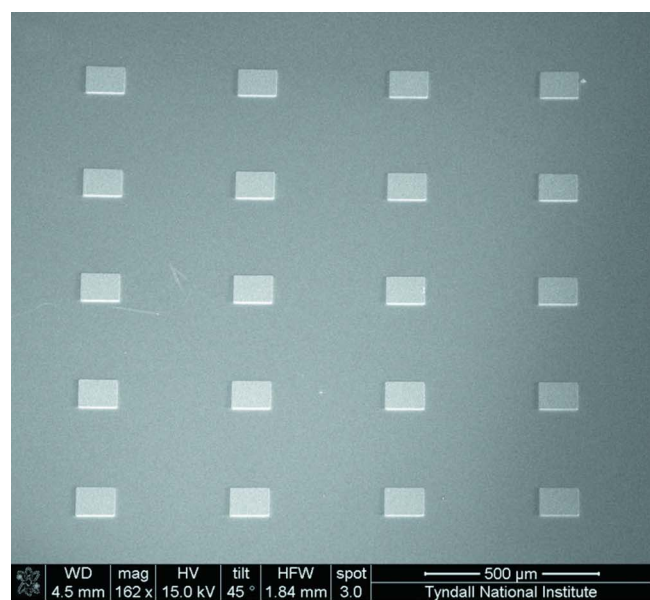
sion coefficient value of  $\text{Cu}^{2+}$  ions is  $6.82 \times 10^{-6} \text{ cm}^2/\text{s}$  [from the initial part of the Cottrell plot ( $I/A$  vs  $1/\sqrt{t}$ ) with a correlation coefficient value of 0.99994]. There is no prior literature available for the diffusion coefficient value of  $\text{Cu}^{2+}$  ions in methanesulfonate solutions. The diffusion coefficient measured for the MSA electrolyte is comparable to the mean literature value of  $7.54 \times 10^{-6} \text{ cm}^2/\text{s}$  cited by Quickenden and Xu<sup>8</sup> for  $\text{Cu}^{2+}$  in sulfate systems.

Figure 5 shows the UV-vis spectrometry of two solutions, where the maximum of the absorption band in the  $\text{CuSO}_4 \cdot 5\text{H}_2\text{O}$  solution is at 810 nm and no shift of the maximum absorption is apparent in the  $\text{Cu}(\text{O}_3\text{SCH}_3)_2 \cdot 4\text{H}_2\text{O}$  solution. This indicates that the Cu species in both electrolytes have the same coordination with respect to surrounding anions and water molecules [ $\text{Cu}(\text{H}_2\text{O})_6$ ]. The high efficiency of the methanesulfonate bath can be interpreted, at least partially, in terms of the methanesulfonate anion acting as an accelerator when added as the Cu salt itself.

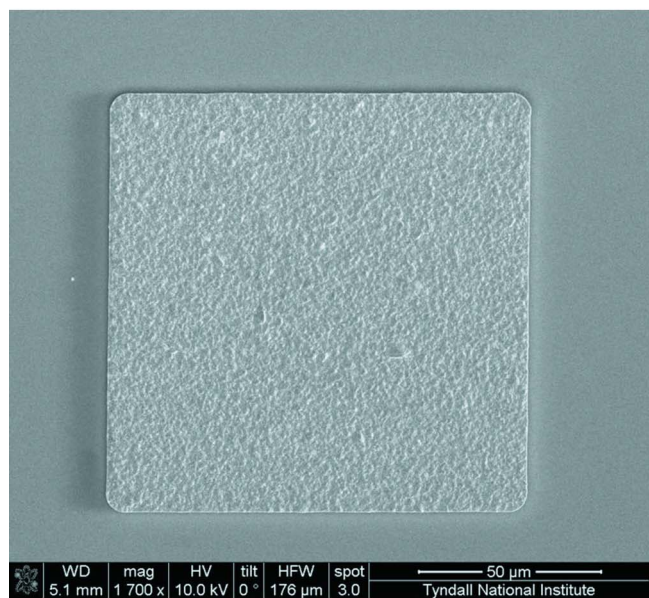
Figure 6a shows a Cu deposit array in a 12  $\mu\text{m}$  thick AZ 9260 photoresist mold after photoresist removal. The experiment demonstrated the chemical stability of the photoresist in the methanesulfonate bath and the Cu electrodeposition efficiency without addi-



**Figure 5.** (Color online) The absorbance as a function of wavelength ( $\lambda$ ) in methanesulfonate (solid line) and sulfate (filled square line) baths.



(a)



(b)

**Figure 6.** (Color online) (a) SEM of Cu micropad array in a 12  $\mu\text{m}$  thick AZ 9260 photoresist mold after resist removal. (b) Magnified single pad showing linear square features with void-free deposit.

tive influence. The Cu was deposited to fill the open structures at 10  $\text{mA}/\text{cm}^2$  for 1 h. The uniformity of the deposited Cu from the MSA electrolyte is shown in Fig. 6b. It can also be seen that the dimension of the developed features is a linear square size, i.e., no sidewall undercutting or voids are observed. Therefore, the photolithography-assisted Cu interconnect fabrication is viable in the MSA electrolyte.

The properties of metallic films differ remarkably from the bulk materials when the thickness of the metallic films decreases to the submicrometer or nanoscale length.<sup>9,10</sup> Here, the electrical resistivity of Cu thin film is estimated using a four-point probe technique according to the following equation

$$\rho = \frac{G(s,t)V}{I} \quad [4]$$

$G$  is the geometric factor, has a unit of length, and is given by the following equation<sup>11</sup>

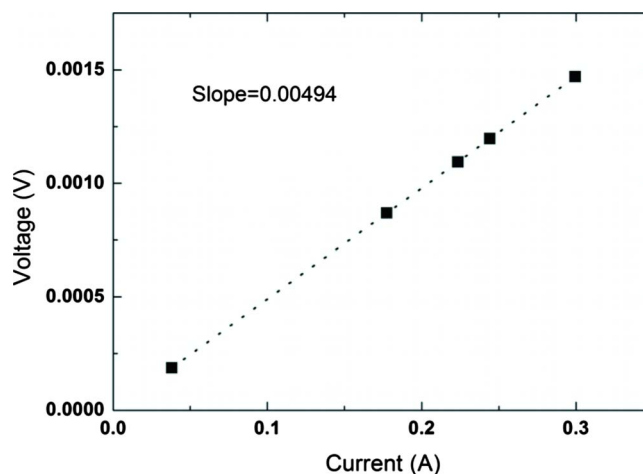


**Figure 7.** (Color online) Sheet resistance curve for 1  $\times$  1 cm square size and 1.02  $\mu\text{m}$  thick Cu film.

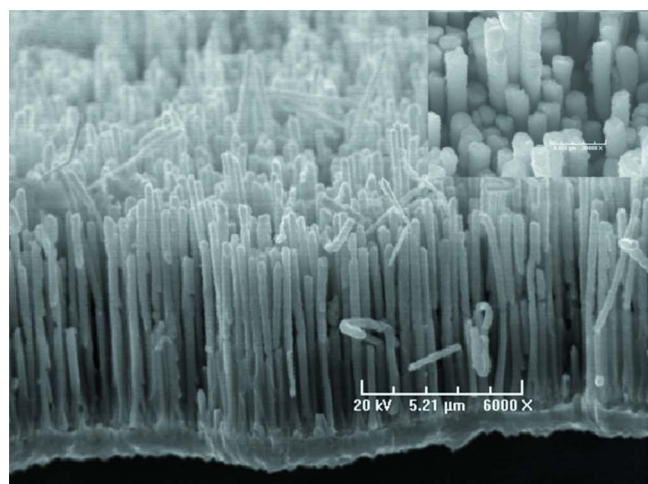
$$G = t \cdot \frac{\pi}{\ln(2)} \cdot C \left( \frac{d}{s}, \frac{a}{d} \right) \quad [5]$$

where  $C$  is the additional correction factor due to the finite dimension of the film,  $a$  and  $d$  are the length and breadth, respectively, and  $s$  is the probe spacing. Figure 7 shows the sheet resistance curve for which current and voltage are linearly proportional. Using the value of  $G$  suggested by Smits,<sup>11</sup> the estimated sheet resistivity is 2.12  $\mu\Omega/\text{cm}$  ( $G = 4.2209$  for  $a = d$ , 10 mm and  $s = 10^{-3}$  m; here  $t = 1.02 \times 10^{-6}$  m, slope = 0.00494  $\Omega/\text{m}$ ); this value is comparable to available literature data.<sup>12</sup>

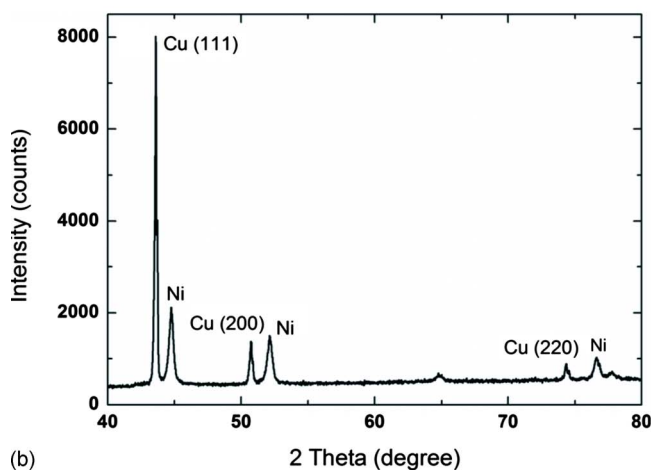
Figure 8a shows the SEM image of the well-ordered and homogeneous growth of Cu nanorod arrays from a bath of 0.24 M  $\text{Cu}(\text{O}_3\text{SCH}_3)_2 \cdot 4\text{H}_2\text{O}$  in 1.8 M  $\text{CH}_3\text{SO}_3\text{H}$ . The average diameter of the Cu nanorods is measured to be 290 nm, which correlates with the value of the pore diameter of the AAO template. The deposition rate is 0.55  $\mu\text{m}/\text{min}$  at 40 mA with an additive-free solution by comparison with the slower deposition rate of 0.32  $\mu\text{m}/\text{min}$ <sup>13</sup> for a Cu sulfate bath operated under the same conditions. When the typical additives such as PEG and  $\text{Cl}^-$  were added to the MSA electrolyte, the templated deposits were solid wires rather than tubes as achieved in the sulfate system described in Ref. 13. Thus, it would appear that the suppression effects of that combination of additives do not govern the deposition type in the MSA bath, and high rate solid structures are achieved. Indeed, it may be that the MSA anion acts as an accelerator for Cu deposition and leads to the enhanced kinetics for deposition observed in voltammetry and chronoamperometry. The XRD pattern reveals that Cu nanorods are polycrystalline, having a preferred orientation of (111); the peaks from the Ni seed layer are also apparent (see Fig. 8b). The preferred crystalline orientation of deposits depend on the conditions of electrodeposition such as current density, bath composition, electrolyte convection, temperature, pH, etc.<sup>14</sup> It has been observed that the increasing cathodic current from 40 to 100 mA or bath temperature from 20 to 40°C resulted in the development of the (200) and (220) orientations at the same pH (0.45).

## Conclusion

MSA has been shown to be a potential electrolyte for Cu electrodeposition. In this paper, we presented a preliminary study of Cu electrodeposition on the GC electrode from the MSA and sulfuric acid electrolytic solutions. The CV results indicate that the overpotential for the Cu deposition is much lower in the methanesulfonate bath. Consequently, from the current transients, it is evident that for a fixed value of the overpotential, the kinetics of Cu nucleation is larger in the MSA bath compared to that in the sulfuric acid bath.



(a)



(b)

**Figure 8.** (Color online) (a) SEM image of Cu nanorod arrays (inset is top view) and (b) XRD patterns of Cu deposit.

The diffusion coefficient for the Cu deposition from MSA is estimated to be  $6.82 \times 10^{-6} \text{ cm}^2/\text{s}$ . The difference in nucleation behavior is most likely due to the difference in the adsorption of the

background electrolyte ions and  $\text{Cu}^{2+}$  on the GC interface surface, where the coordination strength of  $\text{Cu}^{2+}$  ions with the surrounding anions or water molecules influences the formation of a critical nucleus that precedes further growth. The enhanced kinetics and lower overpotential for the Cu electrodeposition using MSA may result from accelerator effects of the MSA by comparison with the sulfuric acid electrolyte.

Void-free Cu deposits have also been fabricated by a through-hole electroplating process on Ni sputtered Si substrates. Cu square pads ( $100 \times 100 \mu\text{m}$ ) with a pitch of  $400 \mu\text{m}$  have been demonstrated. The electrical resistivity of the as-deposited Cu thin film is measured to be  $2.12 \mu\Omega \text{ cm}$ , which correlates with literature values for Cu from sulfate baths. Cu nanorods were also electrodeposited through an AAO template on Ni evaporated substrate to investigate submicrometer deposition from the MSA bath. The Cu methanesulfonate bath is suitable for high rate deposition of void-free Cu micrometer-scale pads and nanorod interconnects for additive-free 3D ULSI and MEMS applications.

#### Acknowledgment

The authors acknowledge Enterprise Ireland Technology Development Project CFTD/05/IT/317. M.H. is grateful for the help of Professor L. Heerman.

University College Cork assisted in meeting the publication costs of this article.

#### References

1. T. P. Moffat, D. Wheeler, W. H. Huber, and D. Josell, *Electrochem. Solid-State Lett.*, **4**, C26 (2001).
2. L. T. Koh, G. Z. You, S. Y. Lim, C. Y. Lim, and P. D. Foo, *Microelectron. J.*, **32**, 973 (2001).
3. R. Akolkar and U. Landau, *J. Electrochem. Soc.*, **151**, C702 (2004).
4. J. J. Kelly and A. C. West, *J. Electrochem. Soc.*, **145**, 3472 (1998).
5. M. D. Gernon, M. Wu, T. Buszta, and P. Janney, *Green Chem.*, **1**, 127 (1999).
6. J. Ma, Y. Kale, and M. Turnbull, Biocatalysis/Biodegradation Database, University of Minnesota (1997).
7. A. J. Bard and L. R. Faulkner, *Electrochemical Methods. Fundamental and Applications*, p. 218, John Wiley & Sons, New York (1980).
8. T. I. Quickenden and Q. Xu, *J. Electrochem. Soc.*, **143**, 1248 (1996).
9. M. D. Uchic, D. M. Dimiduk, J. N. Florando, and W. D. Nix, *Science*, **305**, 986 (2004).
10. Z. P. Bažant, Z. Y. Guo, H. D. Espinosa, Y. Zhu, and B. Peng, *J. Appl. Phys.*, **97**, 073506 (2005).
11. F. M. Smits, *Bell Syst. Tech. J.*, **37**, 711 (1958).
12. P. Dixit, C. W. Tan, L. Xu, N. Lin, J. Miao, J. H. L. Pang, P. Backus, and R. Preisser, *J. Micromech. Microeng.*, **17**, 1078 (2007).
13. T. Chowdhury, D. P. Casey, and J. F. Rohan, *Electrochem. Commun.*, **11**, 1203 (2009).
14. M. Hasan, M.S. Thesis, Katholieke Universiteit Leuven, Belgium (2005).